Performance of LDPC Coded OTFS Systems over High Mobility Channels

ZHANG Chong[1,2,3,4], XING Wang[1,2,3,4], YUAN Jinhong[5], ZHOU Yiqing[1,2,3,4]

(1. Beijing Key Laboratory of Mobile Computing and Pervasive Device, Beijing 100190, China;
2. Institute of Computing Technology, Chinese Academy of Sciences, Beijing 100190, China;
3. University of Chinese Academy of Sciences, Beijing 100049, China;
4. Zhongke Nanjing Mobile Communication & Computing Innovation Institute, Nanjing 211135, China;
5. School of Electrical Engineering and Telecommunications, University of New South Wales, Sydney NSW 2052, Australia)

Abstract: The upcoming 6G wireless networks have to provide reliable communications in high-mobility scenarios at high carrier frequencies. However, high-mobility or high carrier frequencies will bring severe inter-carrier interference (ICI) to conventional orthogonal frequency-division multiplexing (OFDM) modulation. Orthogonal time frequency space (OTFS) modulation is a recently developing multi-carrier transmission scheme for wireless communications in high-mobility environments. This paper evaluates the performance of coded OTFS systems. In particular, we consider 5G low density parity check (LDPC) codes for OTFS systems based on 5G OFDM frame structures over high mobility channels. We show the performance of the OTFS systems with 5G LDPC codes when sum-product detection algorithm and iterative detection and decoding are employed. We also illustrate the effect of channel estimation error on the performance of the LDPC coded OTFS systems.

Keywords: OTFS; LDPC codes; OFDM

DOI: 10.12142/ZTECOM.202104005

https://kns.cnki.net/kcms/detail/34.1294.TN.20211210.1815.002.html, published online December 14, 2021

Manuscript received: 2021-10-29

Citation (IEEE Format): C. Zhang, W. Xing, J. H. Yuan, et al., "Performance of LDPC coded OTFS systems over high mobility channels," *ZTE Communications*, vol. 19, no. 4, pp. 45 - 53, Dec. 2021. doi: 10.12142/ZTECOM.202104005.

1 Introduction

Future wireless networks are expected to provide high-speed and ultra-reliable communication[1-6] for a number of emerging wireless applications, such as the millimeter wave (mmWave) [7], low-earth-orbit satellites (LEOSs)[8], high-speed trains[9], and unmanned aerial vehicles (UAVs)[10]. In practice, one of the challenges for these systems is that wireless communication for high mobility is always accompanied by severe Doppler spread. While orthogonal frequency division multiplexing (OFDM) currently deployed in Long Term Evolution (LTE) and 5G systems can achieve high spectral efficiency for time-varying frequency selective channels, it suffers from heavy performance degradation in high Doppler conditions due to severe Doppler spread. Therefore, new modulation and signal processing techniques that are more robust to time-varying channels are required to meet the challenging requirements of high mobility communications.

Recently, the orthogonal time frequency space (OTFS) modulation proposed in Refs. [11 - 12] has drawn a lot of attention due to its advantages over OFDM in high Doppler channels where each transmitted data symbol can exploit the channel's delay and Doppler variations. OTFS is a two-dimensional (2D) modulation scheme, where the information symbols are modulated into the 2D delay-Doppler (DD) domain rather than into the time-frequency (TF) domain as the classic OFDM modulation. Thus, the time-varying channel in the TF domain can be transformed into a 2D quasi-time-invariant channel in the DD domain, where attractive properties, such as separability, stability, and compactness, can be exploited[12]. With the application of inverse symplectic finite Fourier transform (ISFFT) in OTFS, symbols in the DD domain can be transformed to the TF domain, in which each symbol in the DD domain spans the whole bandwidth and time duration of the transmission frame. Therefore, the OTFS modulation can offer the potential of ex-

This paper was partially supported by National Key R&D Program of China (No. 2020YFB1807802) the National Science Fund for Distinguished Young Scholars (No. 61901453), and Jiangsu Provincial Key Research and Development Program (No. BE2021013-2).
ZHOU Yiqing is the corresponding author.

ploiting the full diversity. However, modulating information symbols into the DD domain makes conventional receiver technologies cannot be applied directly, which in turn requires advanced channel coding, signal estimation and detection methods for OTFS to achieve the potential full diversity and reliable error performance.

Accurately estimating the channel parameters in OTFS systems is a challenging but vital requirement for reliable detection. A simple channel estimation algorithm for OTFS is to embed the pilot signals in the DD domain[13 - 14] to obtain DD channel responses of each transmitting path. This method has low complexity and signal overhead. But it suffers from performance degradation for channels with fractional Doppler. In Ref. [15], the authors proposed a channel estimation method based on pseudo-noise (PN) to estimate the Doppler frequency of each transmitting path, which has high computational complexity to estimate the fractional Doppler. Using deep learning algorithms to assist in the channel estimation has recently been proposed as a potential technology to get more accurate estimation parameters. For example, in Ref. [16], two deep learning assisted algorithms were proposed to facilitate channel estimation for massive machine-type communication, which could potentially be applied to OTFS channel estimation to deal with fractional Doppler.

Many existing studies focus on signal detection for OTFS modulation. In Ref. [17], the authors gave an iterative detection based on the message passing (MP) algorithm. However, the MP detection treats the interference from other information symbols as a Gaussian variable to reduce the detection complexity, which may fail to converge and result in performance degradation. To solve this problem, the authors in Refs. [18 - 19] explored the approximate message passing algorithm. They proposed a detection algorithm by covariance processing to obtain better BER performance in Ref. [18] and a convergence guaranteed receiver based on the variational Bayes framework in Ref. [19]. An OTFS detection approach based on approximate message passing (AMP) with a unitary AMP transformation (UAMP) was developed in Ref. [20], which enjoys the structure of the channel matrix and allows efficient implementation. Inspired by the connection between the orthogonality and message passing, the authors in Ref. [21] proposed a novel cross domain iterative detection algorithm for OTFS modulation, where the extrinsic information is passed between the time domain and DD domain via the corresponding unitary transformations. This algorithm has low computational complexity and can achieve almost the same error performance as the maximum-likelihood sequence detection even in the presence of fractional Doppler shifts.

Most papers focus on the basic principle or key algorithms for the estimation or detection of OTFS systems, while little attention has been paid to coded OTFS systems. The authors in Ref. [22] analyzed coded OTFS performance, but they only considered classical codes, ignoring modern coding technologies like LDPC, Turbo, or Polar codes for OTFS systems, which are important to achieve high reliability and channel capacity. Therefore, we are going to evaluate modern LDPC coded OTFS performance in this work.

In this paper, we first provide a brief overview of the fundamental concepts of OTFS. Then we consider 5G LDPC codes for OTFS systems over high mobility channels. As OTFS can be built on the top of the OFDM frame structure, we also consider the 5G OFDM frame structure in our evaluations. The effect of channel estimation errors on the LDPC coded OTFS system performance is evaluated as well. The rest of this article is organized as follows. Section 2 introduces related knowledge of OTFS including the basic conceptions, system model, OTFS modulation/demodulation, and the channel input-output relationship. In Section 3, we provide an overview of the error performance analysis for OTFS systems. In Section 4, we present the details of the performance evaluation of OTFS systems with 5G LDPC codes. Section 5 concludes the paper.

2 OTFS System

In this section, we first present an OTFS system model. Then, we briefly review the input-output relations for the OTFS systems[11 - 12, 17].

2.1 OTFS System Model

An OTFS modulation is a 2D modulation, which modulates information in the DD domain before transforming signals to TF and time domains. The time-frequency signal plane is discretized to a grid by sampling time and frequency axes at intervals T (s) and Δf (Hz), respectively, i.e.,

$$\Lambda = \left\{\left(nT, m\Delta f\right), n = 0,\ldots,N-1, m = 0,\ldots,M-1\right\}. \tag{1}$$

For some integers $N,M > 0$, where $T = 1/\Delta f$, N and M are the numbers of time and frequency grids, respectively. Therefore, we can obtain that an OTFS frame is transmitted with duration $T_{\text{frame}} = NT$ and occupies a bandwidth $B_{\text{frame}} = M\Delta f$.

Accordingly, let us define the delay-Doppler plane as,

$$\Gamma = \left\{\left(\frac{k}{NT}, \frac{l}{M\Delta f}\right), k = 0,\ldots,N-1, l = 0,\ldots,M-1\right\}, \tag{2}$$

where $\frac{1}{M\Delta f}$ and $\frac{1}{NT}$ represent the quantization steps of the delay and Doppler frequency, respectively. They are also called delay and Doppler resolution.

Let a set $\mathbb{A} = \left\{a_1,\ldots,a_Q\right\}$ denote the constellation alphabet with sized Q and a set of NM modulated symbols $x_0,\ldots,x_{NM-1} \in \mathbb{A}$ to be transmitted by OTFS. The OTFS modulation firstly maps symbols $x_0,\ldots,x_{NM-1}$ to DD plane Γ. Here, we use $x\left[k,l\right], k = 0,\ldots,N-1, l = 0,\ldots,M-1$ to represent the baseband modulated symbols to be transmitted in DD plane, where k

denotes Doppler index and l denotes delay index.

Then, the signal in DD plane Γ is transformed to TF plane Λ, whereby the symbols in DD domain $x[k,l], k = 0,...,N-1, l = 0,...,M-1$ are mapped into TF domain $X[n,m], n = 0,...,N-1, m = 0,...,M-1$, where n denotes the time index and m denotes the frequency index. Such mapping of $x[k,l]$ to $X[n,m]$ can be realized by ISFFT[11].

$$X[n,m] = ISFFT(x[k,l]) = \frac{1}{\sqrt{NM}}\sum_{k=0}^{N-1}\sum_{l=0}^{M-1}x[k,l]e^{j2\pi\left(\frac{nk}{N}-\frac{ml}{M}\right)}. \tag{3}$$

Next, a multi-carrier modulator, such as OFDM, is used to transform the samples $X[n,m]$ at each time slot to a continuous time waveform $s(t)$ with a pulse shaping $g_{tx}(t)$ as the transmitted pulse. Such a transformation can be realized by discrete Heisenberg transform[11],

$$s(t) = \sum_{m=0}^{M-1}\sum_{n=0}^{N-1}X[n,m]e^{j2\pi m\Delta f(t-nT)}g_{tx}(t-nT). \tag{4}$$

The cross-ambiguity function between the transmitted pulse shaping $g_{tx}(t)$ and the received pulse shaping $g_{rx}(t)$ is given by[11]

$$A_{g_{rx},g_{tx}}(t,f) = \int g_{rx}^{*}(t'-t)g_{tx}(t')e^{-j2\pi f(t'-t)}dt'. \tag{5}$$

Here, we only discuss OTFS modulation/demodulation principles without channel effects. Let $r(t)$ denote the received signal. At the receiver, a match filter is applied to compute the cross-ambiguity function $A_{g_{rx},r(t)}(t,f)$ as

$$Y(t,f) = A_{g_{rx},r(t)}(t,f) \triangleq \int g_{rx}^{*}(t'-t)r(t')e^{-j2\pi f(t'-t)}dt'. \tag{6}$$

By sampling $Y(t,f)$ as $Y[n,m] = Y(t,f)|_{t=nT,f=m\Delta f}$, $Y[n,m], n = 0,...,N-1, m = 0,...,M-1$ can be obtained.

Then, by transforming TF plane Λ signal $Y[n,m]$ back to DD plane Γ signal $y[k,l]$ with symplectic finite Fourier transform (SFFT), symbols in DD domain can be recovered as[11]

$$y[k,l] = \mathrm{SFFT}(Y[n,m]) = \frac{1}{\sqrt{NM}}\sum_{n=0}^{N-1}\sum_{m=0}^{M-1}Y[n,m]e^{-j2\pi\left(\frac{nk}{N}-\frac{ml}{M}\right)}. \tag{7}$$

2.2 Input-Output Relations of OTFS Signal

In this subsection, we present the channel model and the input-output relations between the transmitter and the receiver[17]. We assume that only a few reflectors are moving within one OTFS frame duration in practice, and only a small number of channel taps are associated with Doppler shift. Therefore, the channel response of the DD domain is sparse compared with the whole DD plane. Considering a channel with P independent distinguishable paths, the channel response can be represented as

$$h(\tau,\nu) = \sum_{i=1}^{P}h_i\delta(\tau-\tau_i)\delta(\nu-\nu_i), \tag{8}$$

where h_i, τ_i and ν_i denote the channel coefficient, delay and Doppler shift associated with the i-th path, respectively. Without considering additive white Gaussian noise (AWGN), the relation of $s(t)$ and $r(t)$ is given by[17]

$$r(t) = \iint h(\tau,\nu)e^{j2\pi\nu(t-\tau)}s(t-\tau)d\tau d\nu. \tag{9}$$

The relation of $X[n,m]$ and $Y[n,m]$ in TF domain is given by[17]

$$Y[n,m] = \sum_{n'=n-1}^{n}\sum_{m'=0}^{M-1}H_{n,m}[n',m']X[n',m'] = H_{n,m}[n,m]X[n,m] + \sum_{m'=0,m'\neq m}^{M-1}H_{n,m}[n,m']X[n,m'] + \sum_{m'=0}^{M-1}H_{n,m}[n-1,m']X[n-1,m'], \tag{10}$$

in which

$$H_{n,m}[n',m'] = \iint h(\tau,\nu)A_{g_{rx},g_{tx}}((n-n')T-\tau,(m-m')\Delta f-\nu)e^{j2\pi\nu n'T} \times e^{j2\pi(\nu+m'\Delta f)((n-n')T-\tau)}d\tau d\nu. \tag{11}$$

The second term in Eq. (10) is the samples $X[n,m']$ at different frequencies $m' \neq m$, which can be seen as the interference to the current sample $X[n,m]$ in the same time slot n. On the other hand, the third term in Eq. (10) accumulates the interference from the samples $X[n-1,m']$ in the previous time slot $n-1$. Hence, we call the second and third terms as the inter-carrier interference (ICI) and inter-symbol interference (ISI), respectively. It is clear that since the delay spread and Doppler spread, there are severe ICI and ISI in the TF domain.

The relation of $x[k,l]$ and $y[k,l]$ in DD domain is given by[17]

$$y[k,l] \approx \sum_{i=1}^{P}\sum_{q=-N_i}^{N_i}h_i e^{j2\pi\left(\frac{l-l_{\tau_i}}{M}\right)\left(\frac{k_{\nu_i}+\kappa_{\nu_i}}{N}\right)}\alpha_i(k,l,q)x\left[\left[k-k_{\nu_i}+q\right]_N,\left[l-l_{\tau_i}\right]_M\right], \tag{12}$$

where

$$\alpha_i(k,l,q) = \begin{cases} \frac{1}{N}\beta_i(q), & l_{\tau_i} \leqslant l < M \\ \frac{1}{N}(\beta_i(q)-1)e^{-j2\pi\frac{\left[k-k_{\nu_i}+q\right]_N}{N}}, & 0 \leqslant l < l_{\tau_i}, \end{cases}$$

$$\beta_i(q)=\frac{e^{-j2\pi\left(-q-\kappa_{\nu_i}\right)}-1}{e^{-j\frac{2\pi}{N}\left(-q-\kappa_{\nu_i}\right)}-1}$$

and

In Eq. (12), h_i denotes the channel coefficient and N_i is the number of neighboring transmitted signals in the Doppler domain, where $0<N_i\ll N$. The l_{τ_i} and k_{ν_i} are the delay and Doppler indices corresponding to the i-th path, respectively, and we have

$$\tau_i=\frac{l_{\tau_i}}{M\Delta f},\ \nu_i=\frac{k_{\nu_i}+\kappa_{\nu_i}}{NT}. \tag{13}$$

Note that the term $-\frac{1}{2}<\kappa_{\nu_i}\leqslant\frac{1}{2}$ denotes the fractional Doppler shifts which correspond to the fractional shifts from the nearest Doppler indices[17]. For wideband systems, the typical value of the sampling time in the delay domain is usually sufficiently small. Therefore, the impact of fractional delays in typical wide-band systems can be neglected[24]. Here, we have $-k_{\max}\leqslant k_i+\kappa_i\leqslant k_{\max}$, where $k_{\max}$ is the maximum Doppler index satisfying $k_{\max}=\lceil NT\nu_{\max}\rceil$[17].

From Eq. (12), we can see that the received signal $y[k,l]$ is a linear combination of $S=\sum_{i=1}^{P}2N_i+1$ transmitted signals. The signal corresponding to $q=0$, $x\left[[k-k_{\nu_i}]_N,[l-l_{\tau_i}]_M\right]$ contributes the most, and all the other $2N_i$ signals can be seen as interference. Such interference is due to the transmitted signals neighboring $x\left[[k-k_{\nu_i}]_N,[l-l_{\tau_i}]_M\right]$ in the Doppler domain caused by fractional Doppler and we refer to this interference as inter-Doppler interference (IDI). In the TF domain, the delay spread and Doppler spread cause severe ICI and ISI as the second and the third terms in Eq. (10), which are hard to distinguish in the received signals. However, in the DD domain, they mainly affect the phase shifts as $e^{j2\pi\left(\frac{l-l_{\tau_i}}{M}\right)\left(\frac{k_{\nu_i}+\kappa_{\nu_i}}{N}\right)}$.

Now, let us represent the DD domain input-output relation in a vector form. Let $\boldsymbol{x}\triangleq\mathrm{vec}(\boldsymbol{X})\in\mathbb{A}^{MN}$ and $\boldsymbol{y}\triangleq\mathrm{vec}(\boldsymbol{Y})\in\mathbb{A}^{MN}$ denote the vector forms of the transmitted symbols X and the received symbols Y in DD domain, respectively. According to Eq. (9), we have

$$\boldsymbol{y}=\boldsymbol{H}_{\mathrm{eff}}\boldsymbol{x}+\boldsymbol{w}, \tag{14}$$

where $\boldsymbol{w}$ is the corresponding noise vector and $\boldsymbol{H}_{\mathrm{eff}}$ of size $MN\times MN$ is the effective channel matrix in the DD domain. Assuming that both $g_{tx}(t)$ and $g_{rx}(t)$ are rectangular pulses, with a reduced CP frame format, the effective channel matrix $\boldsymbol{H}_{\mathrm{eff}}$ is given by[23]

$$\boldsymbol{H}_{\mathrm{eff}}=\sum_{i=1}^{P}h_i\left(\boldsymbol{F}_N\otimes\boldsymbol{I}_M\right)\boldsymbol{\Pi}^{l_{\tau_i}}\Delta^{\left(k_{\nu_i}+\kappa_{\nu_i}\right)}(\boldsymbol{F}_N^{\mathrm{H}}\otimes\boldsymbol{I}_M), \tag{15}$$

where $\boldsymbol{\Pi}$ is the permutation matrix (forward cyclic shift), i.e.,

$$\boldsymbol{\Pi}=\begin{bmatrix}0&0&\cdots&0&0\\1&\ddots&\ddots&\ddots&0\\\vdots&1&0&\ddots&\vdots\\0&\ddots&\ddots&\ddots&0\\0&0&\cdots&1&0\end{bmatrix}_{MN\times MN}, \tag{16}$$

and Δ is a diagonal matrix,

$$\Delta=\mathrm{diag}\{e^{j2\pi\frac{0}{NM}},e^{j2\pi\frac{1}{NM}},\ldots,e^{j2\pi\frac{NM-1}{NM}}\}. \tag{17}$$

3 Error Performance Analysis

In this section, we discuss the error performance of the uncoded and coded OTFS systems, respectively. We assume that ideal channel state information (CSI) is available at the receiver.

3.1 Uncoded OTFS System Performance

According to Ref. [26], Eq. (14) can be rewritten as

$$\boldsymbol{y}=\boldsymbol{\Phi}_{\tau,\nu}(\boldsymbol{x})\boldsymbol{h}+\boldsymbol{w}, \tag{18}$$

where $\boldsymbol{\Phi}_{\tau,\nu}(\boldsymbol{x})$ is referred to as the equivalent code-word matrix and it is a concatenated matrix of size $MN\times P$ constructed by the column vector $\boldsymbol{\Xi}_i\boldsymbol{x}$, i.e.,

$$\boldsymbol{\Phi}_{\tau,\nu}(\boldsymbol{x})=\left[\boldsymbol{\Xi}_1\boldsymbol{x}\,\boldsymbol{\Xi}_2\boldsymbol{x},\ldots,\boldsymbol{\Xi}_P\boldsymbol{x}\right], \tag{19}$$

and $\boldsymbol{\Xi}_i$ is given by

$$\boldsymbol{\Xi}_i\triangleq\left(\boldsymbol{F}_N\otimes\boldsymbol{I}_M\right)\Pi^{l_{\tau_i}}\Delta^{\left(k_i+\kappa_i\right)}(\boldsymbol{F}_N^{\mathrm{H}}\otimes\boldsymbol{I}_M),1\leqslant i\leqslant P. \tag{20}$$

In Eq. (18), $\boldsymbol{h}$ is the channel coefficient vector of size $P\times 1$, i.e., $\boldsymbol{h}=\left[h_1,h_2,\ldots,h_P\right]^T$, where the elements in $\boldsymbol{h}$ are assumed to be independently and identically distributed complex Gaussian random variables. Besides, we assume a uniform power delay and Doppler profile of the channel so that the channel coefficient h_i has mean μ and variance $1/2P$ per real dimension for $1\leqslant i\leqslant P$ and is independent from the delay and Doppler indices[25]. In particular, we note that if $\mu=0$, h_i follows the Rayleigh distribution, which will be considered as a special case in the error performance analysis and code design.

Based on Eq. (18), for a given channel realization, we define the conditional Euclidean distance $d^2_{h,\tau,\nu}(\boldsymbol{x},\boldsymbol{x}')$ between a pair of code-words $\boldsymbol{x}$ and $\boldsymbol{x}'(\boldsymbol{x}\neq\boldsymbol{x}')$ as

$$d^2_{h,\tau,\nu}(\boldsymbol{x},\boldsymbol{x}')=d^2_{h,\tau,\nu}(\boldsymbol{e})\triangleq\|\boldsymbol{\Phi}_{\tau,\nu}(\boldsymbol{e})\boldsymbol{h}\|^2=\boldsymbol{h}^{\mathrm{H}}\boldsymbol{\Omega}_{\tau,\nu}(\boldsymbol{e})\boldsymbol{h}, \tag{21}$$

where $\boldsymbol{e}=\boldsymbol{x}-\boldsymbol{x}'$ is the corresponding code-word difference (error) sequence and $\boldsymbol{\Omega}_{\tau,\nu}(\boldsymbol{e})=\left(\boldsymbol{\Phi}_{\tau,\nu}(\boldsymbol{e})\right)^{\mathrm{H}}\left(\boldsymbol{\Phi}_{\tau,\nu}(\boldsymbol{e})\right)$ is referred to as the code-word difference matrix. Here we have

$$\boldsymbol{\Omega}_{\tau,\nu}(\boldsymbol{e})=\begin{bmatrix} \mathrm{e}^{\mathrm{H}}\Xi_1^{\mathrm{H}}\Xi_1\mathrm{e} & \mathrm{e}^{\mathrm{H}}\Xi_1^{\mathrm{H}}\Xi_2\mathrm{e} & \cdots & \mathrm{e}^{\mathrm{H}}\Xi_1^{\mathrm{H}}\Xi_P\mathrm{e} \\ \mathrm{e}^{\mathrm{H}}\Xi_2^{\mathrm{H}}\Xi_1\mathrm{e} & \mathrm{e}^{\mathrm{H}}\Xi_2^{\mathrm{H}}\Xi_2\mathrm{e} & & \vdots \\ \vdots & & \ddots & \vdots \\ \mathrm{e}^{\mathrm{H}}\Xi_P^{\mathrm{H}}\Xi_1\mathrm{e} & \cdots & \cdots & \mathrm{e}^{\mathrm{H}}\Xi_P^{\mathrm{H}}\Xi_P\mathrm{e} \end{bmatrix}. \quad (22)$$

Note that the code-word difference matrix $\boldsymbol{\Omega}(\boldsymbol{e})$ is positive semidefinite Hermitian with a rank r, where $r \leqslant P$. Let us denote by $\{\boldsymbol{v}_1,\boldsymbol{v}_2,...,\boldsymbol{v}_P\}$ the eigenvectors of $\boldsymbol{\Omega}(\boldsymbol{e})$ and $\{\lambda_1,\lambda_2,...,\lambda_P\}$ the corresponding nonnegative real eigenvalues sorted in the descending order, where $\lambda_i > 0$ for $1 \leqslant i \leqslant r$ and $\lambda_i = 0$ for $r+1 \leqslant i \leqslant P$. Thus, the conditional pairwise-error probability (PEP)[27 - 28] is upper-bounded by

$$\Pr(\boldsymbol{x},\boldsymbol{x}'|\boldsymbol{h},\tau,\nu) \leqslant \exp\left(-\frac{E_s}{4N_0}\sum_{i=1}^{r}\lambda_i\left|\tilde{h}_i\right|^2\right), \quad (23)$$

where E_s is the average symbol energy and $\tilde{h}_i = h_i \cdot v_i$, for $1 \leqslant i \leqslant r$. It can be shown that $\{\tilde{h}_1,\tilde{h}_2,...,\tilde{h}_r\}$ are independent complex Gaussian random variables with mean $\mu_{\tilde{h}_i} = \mathbb{E}[h] \cdot v_i$ and $1/2\,P$ variance per real dimension. It has been defined in the previous work[26, 29 - 30] that the rank of $\boldsymbol{\Omega}(\boldsymbol{e})$ is the diversity gain of the uncoded OTFS system. Specifically, it has been shown in Ref. [30] that the diversity gain of uncoded OTFS modulation systems can be one but the full diversity can be obtained by suitable precoding schemes. Furthermore, Ref. [26] has shown that the full diversity can be achieved almost surely for the case of $P = 2$ when the frame size is sufficiently large, even for uncoded OTFS modulation systems.

3.2 Coded OTFS System Performance

Based on the previous analysis, Ref. [22] gave the error performance of the coded OTFS systems. With the assumptions of the wide-sense stationary-uncorrelated scattering (WSSUS) channel and Rayleigh fading, Eq. (23) can be further simplified as

$$\Pr(\boldsymbol{x},\boldsymbol{x}'|\tau,\nu) \leqslant \left(\prod_{i=1}^{r}\lambda_i/P\right)^{-1}\left(\frac{E_s}{4N_0}\right)^{-r} = \frac{1}{\prod_{i=1}^{r}\lambda_i}\left(\frac{E_s}{4N_0P}\right)^{-r}, \quad (24)$$

and it is approximated by

$$\Pr(\boldsymbol{x},\boldsymbol{x}') \approx \left(\frac{d_{\mathrm{E}}^2(\mathbf{e})}{P}\right)^{-r}\left(\frac{E_s}{4N_0}\right)^{-r}. \quad (25)$$

Based on Eq. (25), we note that the unconditional PEP for OTFS modulation only depends on $d_{\mathrm{E}}^2(\mathbf{e})$, the rank of $\boldsymbol{\Omega}(\boldsymbol{e})$, and the number of independent resolvable paths P, and is independent of the specific distribution of delay and Doppler indices. The power of the signal-to noise ratio (SNR) is referred to as the diversity gain, and the term $d_{\mathrm{E}}^2(\boldsymbol{e})/P$ is referred to as the coding gain, which characterizes the approximate improvement of coded OTFS systems over the uncoded counterpart with the same diversity gain, i.e., the same exponent $-r$[27]. Considering the total diversity, there exists a fundamental trade-off between the diversity gain and the coding gain. Based on the previous work[26, 29 - 30], we can notice that the diversity gain depends on the number of independent resolvable paths P. When P (the rank of $\boldsymbol{\Omega}(\boldsymbol{e})$) is small, the diversity gain is small. It is crucial for OTFS systems that using an optimized channel code can greatly improve the error performance. For a large value of P and a reasonably high SNR, the unconditional PEP of OTFS systems can be approximately upper-bounded[22] by

$$\Pr(\boldsymbol{x},\boldsymbol{x}') \leqslant \exp\left(-\frac{E_s}{16N_0}d_{\mathrm{E}}^2(\boldsymbol{e})\right). \quad (26)$$

Form Eq. (26), we can notice that the channel with a large number of diversity paths approaches an AWGN model[35], which indicates that it is reasonable to use coding gain approximation for AWGN channels for evaluating the coding gain of OTFS systems with a large P. A preliminary guideline for the code design of the OTFS systems is to maximize the minimum value of $d_{\mathrm{E}}^2(\mathbf{e})$ among all pairs of code-words of the code. Note that, the error performance of coded OTFS systems still depends on the channel parameters, which is widely observed in the system design for fading channels[36].

4 Evaluation of Coded OTFS with 5G LDPC Codes

In this section, we provide the performance evaluation of the coded OTFS with 5G LDPC codes. Without loss of generality, we consider the sum-product algorithm (SPA)[31] or message passing algorithm for detection, where the details can be found in Refs. [17, 32]. In specific, we consider 5 MHz channelbandwidth[1] and 15 kHz sub-carrier for a time slot. Followed by a 5G frame structure, 5 MHz channel bandwidth contains 4.5 MHz efficient bandwidth with 300 sub-carriers and a time slot contains 14 OFDM symbols[33], where $N = 14$ and $M = 300$. In all simulations, we consider the Rayleigh fading case. If not otherwise specified, we only consider the integer delay and Doppler case and set the maximum delay index as $l_{\max} = 4$ and the maximum Doppler index as $k_{\max} = 4$. For each channel realization, we randomly select the delay and Doppler indices according to the uniform distribution, so that we have $-k_{\max} \leqslant k_{\nu_i} \leqslant k_{\max}$ and $0 \leqslant l_{\tau_i} \leqslant l_{\max}$. We first present the performance for uncoded OTFS systems with SPA detec-

1 It contains efficient bandwidth and guard band in the 5G frame structure.

tion. Then, we discuss the performance of coded OTFS systems with 5G LDPC codes.

4.1 Uncoded OTFS System via SPA Detection

In Fig. 1, it shows the receiver of the uncoded OTFS system via the iterative SPA detection. The SPA detector needs to iterate the soft information between the detector and the demodulator.

The block-error-rate (BLER) performance of the uncoded OTFS systems with $P = 4$ is shown in Fig. 2. Here, we compare the BLER performance under different iterations. In Fig. 2, "ite × n" means n iterations in the iterative detections. It can be observed that SPA detection can achieve better performance with iterations. For BPSK modulation, increasing the iteration number over two does not provide much improvement. The same phenomenon for QPSK modulation is observed for over four iterations. We notice that there is a trade-off between the numbers of iterations and BLER performance. For higher order modulation, we need more iterations for better performance.

4.2 Coded OTFS System via SPA Detection

Here, we provide performance evaluation of coded OTFS based on 5G LDPC codes[34]. The decoder uses the sum-product decoding algorithm with a floating value, and the maximum decoding iteration number is 50. We show the coded OTFS performance for various modulation and different code lengths.

Fig. 3 shows the receiver of the coded OTFS system via iterative SPA detection. We firstly only consider iterative detection in the coded OTFS system. The received symbols after the OTFS demodulation will be put into the SPA detector. The SPA detector gives soft bit messages corresponding to the received symbols to the demodulator. Soft bit messages after demodulation will back to the SPA detector via the detection iteration loop. After several iterations, soft bit messages will be sent to the decoder for decoding. Compared with Fig. 1, Fig. 3 adds the function of coding and decoding.

Fig. 4 shows the BLER performance of the OTFS systems with $P = 4$. We list the parameters of the codes we use in Table 1. Here, K is the information bit length and R is the code rate. We can observe that for the BPSK modulation, increasing the iteration number does not provide much improvement. For the QPSK modulation, two iterations can obtain better performance. For 16QAM modulation, four iterations can obtain larger performance gain. We notice that there exists an optimal iteration number for different modulations.

Next, we only consider the decoding iteration shown in Fig. 5, where we can notice that the detection iteration loop is replaced by decoding iteration loop. Here, the soft bit messages after demodulation will be straightly sent to the decoder. After decoding, the soft bit messages will be passed to the SPA detector via the decoding iteration loop.

We compare the BLER performance with iterative detection

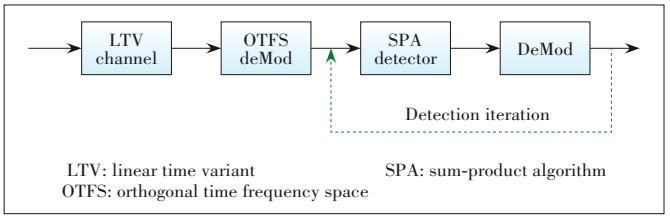

▲Figure 1. An illustration of uncoded OTFS system via iterative SPA detection

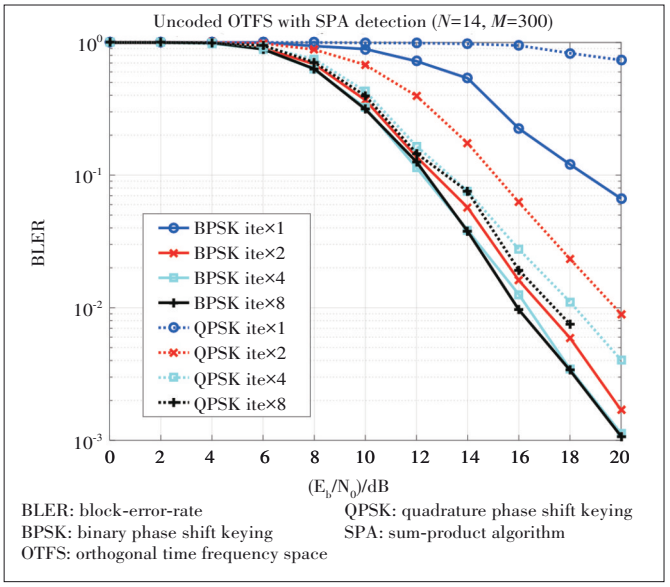

▲Figure 2. BLER performance of the uncoded OTFS systems with P=4

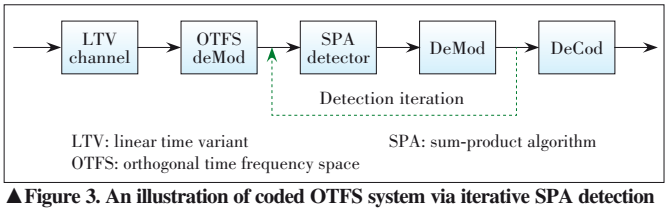

▲Figure 3. An illustration of coded OTFS system via iterative SPA detection

only and with iterative detection-decoding in Figs. 6 and 7. For the BPSK modulation in Fig. 6, the performances are similar.

For the QPSK modulation in Fig. 7, we notice that the performance of the iterative detection is better than that of the iterative detection-decoding.

Here, conducting two and four iterative detections outperforms the iterative decoding at BLER 10^{-2}, with about 0.8 dB and 0.6 dB more gain, respectively. We can notice here that conducting iterative detections can improve the performance more than only iterating between decoding and detection.

Now, we consider the hybrid iterative decoding and detection. In Fig. 8, we have two iteration links. For detection iteration loop (we call it the inner iterative layer), we do SPA detection and demodulation as shown in Fig. 3. For decoding iteration loop (we call it the outer iterative layer), we do decoding and SPA detection as shown in Fig. 5. After several inner iterations, the demodulator sends the soft bit messages to the decoder for decoding, and after decoding, the soft bit messag-

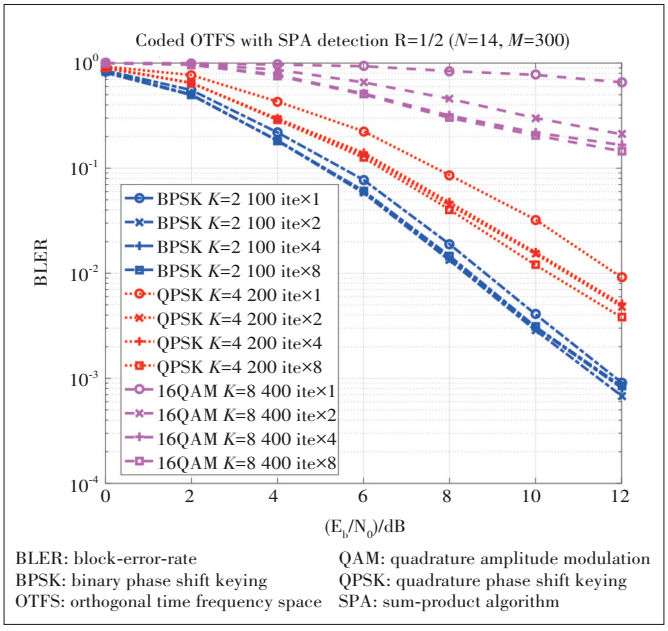

▲Figure 4. BLER performance of the coded OTFS systems

▼Table 1. Parameters of LDPC codes

Information Bits K	Code Rate R	Modulation
2 100	1/2	BPSK
4 200	1/2	QPSK
8 400	1/2	16QAM

BPSK: binary phase shift keying
QPSK: quadrature phase shift keying
QAM: quadrature amplitude modulation

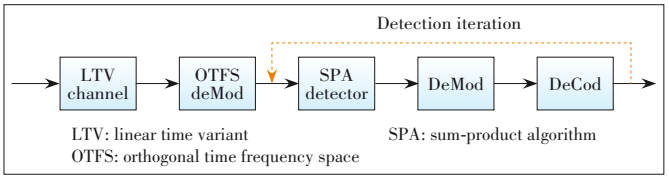

▲Figure 5. Illustration of coded OTFS system via decoding iteration

es will be sent back to the SPA detector via the outer iterative layer. Here, "ite 2 × 2" means doing two decoding iterations and in each decoding iteration there are two detection iterations. In Fig. 9, we can observe that for the BPSK modulation, doing hybrid iterative decoding and detection cannot obtain much gain. For the QPSK modulation, the performance of "ite 2 × 2" hybrid iteration can approach the performance of doing 8 iterative detections. For 16QAM modulation, the performance of "ite 2 × 2" hybrid iterative decoding and detection is similar to the performance of doing 8 iterative detections.

Consequently, we have some observations for coded OTFS systems as follows. For the iterative SPA detection, the optimal iterative numbers depend on the modulation order. Higher order modulation needs a higher number of iterations. Only iterating between decoding and detection does not improve the performance much. Hybrid iterative decoding and detection can achieve better performance, especially for higher order

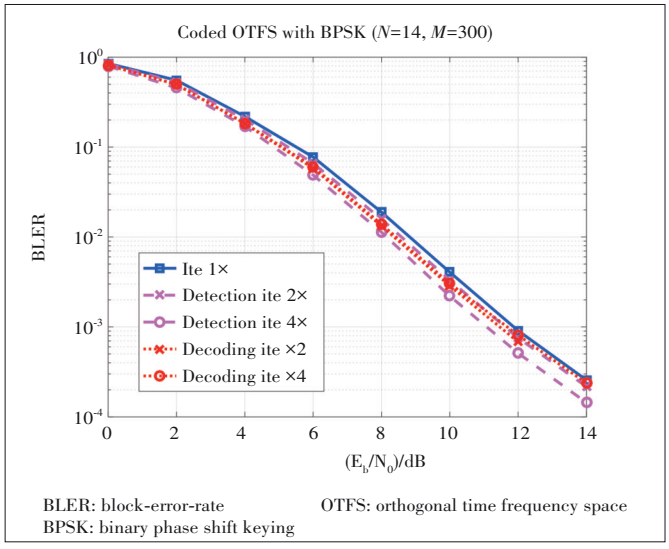

▲Figure 6. BLER performance of the coded OTFS systems with BPSK modulation

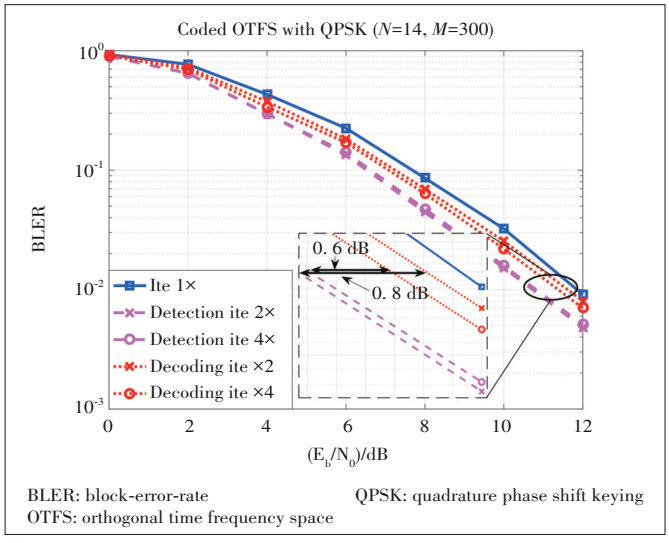

▲Figure 7. BLER performance of the coded OTFS systems with QPSK modulation

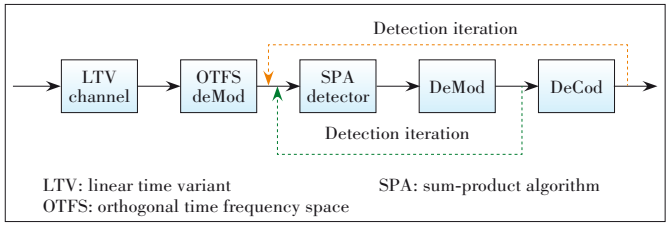

▲Figure 8. An illustration of coded OTFS system via hybrid iteration

modulations.

4.3 Effect of Channel Estimation on Coded OTFS System

Furthermore, we consider the OTFS performance with the channel estimation, where the DD domain channel estimation is employed[14]. In Fig. 10, we compare the performances of uncoded OTFS and coded OTFS system with the channel estimation. Here, we only consider the QPSK modulation with SPA

detection, where the iteration number is 2. "Pilot 30 dB" means the SNR of the pilot is 30 dB. We can see from the figure that the channel estimation has more impact on the performance of the uncoded system than that of the coded OTFS system. For example, the performance gap between "Pilot 30 dB" and "Pilot 40 dB" of the uncoded OTFS system is about 2 dB. For the coded OTFS system, the performance gap between "pilot 30 dB" and "pilot 40 dB" is about 1 dB. In other words, the channel codes reduce the effect of channel estimation on the system. However, the performance of the coded OTFS system shows an error floor below BLER at 10^{-2}, particularly at high SNR due to the channel estimation error.

5 Conclusions

OTFS has great potential in providing reliable communications for next generation wireless communication systems. In this paper, we gave a brief overview of the fundamental concept of OTFS and presented the coded OTFS performance based on 5G LDPC codes. We showed the BLER performance of uncoded OTFS system and coded OTFS system over high mobility channels, and discussed three different coded OTFS schemes with iterative detection and decoding. We also evaluated the impact of channel estimation on the performance of coded OTFS systems.

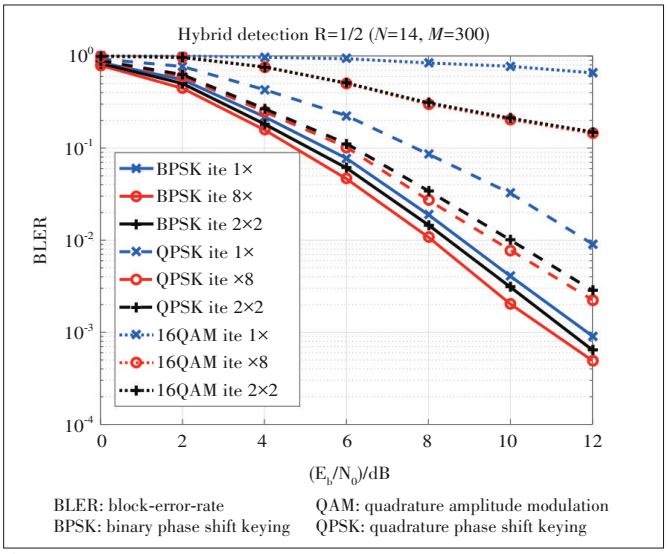

▲ **Figure 9. BLER performance of the coded OTFS systems via hybrid detection and decoding OTFS**

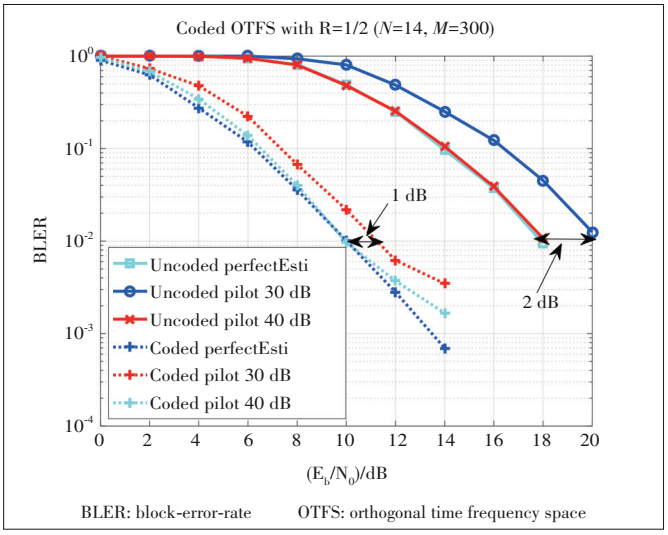

▲ **Figure 10. BLER performance of the coded OTFS systems with channel estimation**

References

[1] ZHOU Y Q, LIU L, WANG L, et al. Service-aware 6G: an intelligent and open network based on the convergence of communication, computing and caching [J]. Digital communications and networks, 2020, 6(3): 253 – 260. DOI: 10.1016/j.dcan.2020.05.003

[2] ZHOU Y Q, TIAN L, LIU L, et al. Fog computing enabled future mobile communication networks: a convergence of communication and computing [J]. IEEE communications magazine, 2019, 57(5): 20 – 27. DOI: 10.1109/MCOM.2019.1800235

[3] LIU L, ZHOU Y Q, YUAN J H, et al. Economically optimal MS association for multimedia content delivery in cache-enabled heterogeneous cloud radio access networks [J]. IEEE journal on selected areas in communications, 2019, 37(7): 1584 – 1593. DOI: 10.1109/JSAC.2019.2916280

[4] LIU L, ZHOU Y Q, ZHUANG W H, et al. Tractable coverage analysis for hexagonal macrocell-based heterogeneous UDNs with adaptive interference-aware CoMP [J]. IEEE transactions on wireless communications, 2019, 18(1): 503 – 517. DOI: 10.1109/TWC.2018.2882434

[5] LIU L, ZHOU Y Q, GARCIA V, et al. Load aware joint CoMP clustering and inter-cell resource scheduling in heterogeneous ultra-dense cellular networks [J]. IEEE transactions on vehicular technology, 2018, 67(3): 2741 – 2755. DOI: 10.1109/TVT.2017.2773640

[6] GARCIA V, ZHOU Y Q, SHI J L. Coordinated multipoint transmission in dense cellular networks with user-centric adaptive clustering [J]. IEEE transactions on wireless communications, 2014, 13(8): 4297 – 4308. DOI: 10.1109/TWC.2014.2316500

[7] JAMEEL F, WYNE S, NAWAZ S J, et al. Propagation channels for mmWave vehicular communications: state-of-the-art and future research directions [J]. IEEE wireless communications, 2019, 26(1): 144 – 150. DOI: 10.1109/MWC.2018.1800174

[8] SU Y T, LIU Y Q, ZHOU Y Q, et al. Broadband LEO satellite communications: architectures and key technologies [J]. IEEE wireless communications, 2019, 26(2): 55 – 61. DOI: 10.1109/MWC.2019.1800299

[9] NOH G, HUI B, KIM I. High speed train communications in 5G: Design elements to mitigate the impact of very high mobility [J]. IEEE wireless communications, 2020, 27(6): 98 – 106. DOI: 10.1109/MWC.001.2000034

[10] BAI L, HAN R, LIU J W, et al. Air-to-ground wireless links for high-speed UAVs [J]. IEEE journal on selected areas in communications, 2020, 38(12): 2918 – 2930. DOI: 10.1109/JSAC.2020.3005471

[11] HADANI R, RAKIB S, TSATSANIS M, et al. Orthogonal time frequency space modulation[C]//2017 IEEE Wireless Communications and Networking Conference (WCNC). San Francisco, USA: IEEE, 2017: 1 – 6. DOI: 10.1109/WCNC.2017.7925924

[12] WEI Z Q, YUAN W J, LI S Y, et al. Orthogonal time-frequency space modulation: a promising next-generation waveform [J]. IEEE wireless communications, 2021, 28(4): 136 – 144. DOI: 10.1109/MWC.001.2000408

[13] HEBRON Y, RAKIB S, HADANI R, et al. Channel acquisition using orthogonal time frequency space modulated pilot signals: PCT/US20 17/025 166 [P]. 2016

[14] RAVITEJA P, PHAN K T, HONG Y. Embedded pilot-aided channel estimation for OTFS in delay – Doppler channels [J]. IEEE transactions on vehicular technology, 2019, 68(5): 4906 – 4917. DOI: 10.1109/TVT.2019.2906357

[15] MURALI K R, CHOCKALINGAM A. On OTFS modulation for high-Doppler

fading channels [J]. 2018 information theory and applications workshop (ITA), 2018: 1 – 10. DOI: 10.1109/ITA.2018.8503182
[16] LIU B, WEI Z Q, YUAN W J, et al. Channel estimation and user identification with deep learning for massive machine-type communications [J]. IEEE transactions on vehicular technology, 2021, 70(10): 10709 – 10722. DOI: 10.1109/TVT.2021.3111081
[17] RAVITEJA P, PHAN K T, HONG Y, et al. Interference cancellation and iterative detection for orthogonal time frequency space modulation [J]. IEEE transactions on wireless communications, 2018, 17(10): 6501 – 6515. DOI: 10.1109/TWC.2018.2860011
[18] LI L J, LIANG Y, FAN P Z, et al. Low complexity detection algorithms for OTFS under rapidly time-varying channel [C]//2019 IEEE 89th Vehicular Technology Conference (VTC2019-Spring). Kuala Lumpur, Malaysia: IEEE, 2019: 1 – 5. DOI: 10.1109/VTCSpring.2019.8746420
[19] YUAN W J, WEI Z Q, YUAN J H, et al. A simple variational Bayes detector for orthogonal time frequency space (OTFS) modulation [J]. IEEE transactions on vehicular technology, 2020, 69(7): 7976 – 7980. DOI: 10.1109/TVT.2020.2991443
[20] YUAN Z D, LIU F, YUAN W J, et al. Iterative detection for orthogonal time frequency space modulation with unitary approximate message passing [J]. IEEE transactions on wireless communications, 7173, (99): 1. DOI: 10.1109/TWC.2021.3097173
[21] LI S Y, YUAN W J, WEI Z Q, et al. Cross domain iterative detection for orthogonal time frequency space modulation [J]. IEEE transactions on wireless communications, 0125, (99): 1. DOI: 10.1109/TWC.2021.3110125
[22] LI S Y, YUAN J H, YUAN W J, et al. Performance analysis of coded OTFS systems over high-mobility channels [J]. IEEE transactions on wireless communications, 2021, 20(9): 6033 – 6048. DOI: 10.1109/TWC.2021.3071493
[23] RAVITEJA P, HONG Y, VITERBO E, et al. Practical pulse-shaping waveforms for reduced-cyclic-prefix OTFS [J]. IEEE transactions on vehicular technology, 2019, 68(1): 957 – 961. DOI: 10.1109/TVT.2018.2878891
[24] TSE D, VISWANATH P. Fundamentals of wireless communication [M]. Cambridge: Cambridge University Press, 2005. DOI: 10.1017/cbo9780511807213
[25] MOLISCH A F. Wireless communications [M]. Hoboken, USA: John Wiley & Sons, 2012
[26] RAVITEJA P, HONG Y, VITERBO E, et al. Effective diversity of OTFS modulation [J]. IEEE wireless communications letters, 2020, 9(2): 249 – 253. DOI: 10.1109/LWC.2019.2951758
[27] TAROKH V, SESHADRI N, CALDERBANK A R. Space-time codes for high data rate wireless communication: Performance criterion and code construction [J]. IEEE transactions on information theory, 1998, 44(2): 744 – 765. DOI: 10.1109/18.661517
[28] VUCETIC B, YUAN J H. Space-time coding [M]. Chichester, UK: John Wiley & Sons, Ltd, 2003. DOI:10.1002/047001413x
[29] BIGLIERI E, RAVITEJA P, HONG Y. Error performance of orthogonal time frequency space (OTFS) modulation [C]//IEEE International Conference on Communications Workshops. Shanghai, China: IEEE, 2019: 1 – 6. DOI: 10.1109/ICCW.2019.8756831
[30] SURABHI G D, AUGUSTINE R M, CHOCKALINGAM A. On the diversity of uncoded OTFS modulation in doubly-dispersive channels [J]. IEEE transactions on wireless communications, 2019, 18(6): 3049 – 3063. DOI: 10.1109/TWC.2019.2909205
[31] KSCHISCHANG F R, FREY B J, LOELIGER H A. Factor graphs and the sum-product algorithm [J]. IEEE transactions on information theory, 2001, 47(2): 498 – 519. DOI: 10.1109/18.910572
[32] LI S Y, YUAN W J, WEI Z Q, et al. Hybrid MAP and PIC detection for OTFS modulation [J]. IEEE transactions on vehicular technology, 2021, 70(7): 7193 – 7198. DOI: 10.1109/tvt.2021.3083181
[33] 3GPP. Technical specification group radio access network: 3GPP TS 38.214 V15.0.0 [S]. 2017
[34] 3GPP. Technical specification group radio access network: 3GPP TS 38.212 V15.0.0 [S]. 2017
[35] VENTURA-TRAVESET J, CAIRE G, BIGLIERI E, et al. Impact of diversity reception on fading channels with coded modulation. Part I: coherent detection [J]. IEEE transactions on communications, 1997, 45(5): 563 – 572. DOI: 10.1109/26.592556
[36] BIGLIERI E, PROAKIS J, SHAMAI S. Fading channels: Informationtheoretic and communications aspects [J]. IEEE transactions on information theory, 1998, 44(6):2619 – 2692

Biographies

ZHANG Chong (zhangchong@ict.ac.cn) received the B.S. degree in electronic & information engineering from Huaqiao University, China in 2017, and the M.S. degree in electronic and communication engineering from University of Chinese Academy of Science, China in 2020. He is currently pursuing the Ph.D. degree in the Institute of Computing Technology, Chinese Academy of Science, China. His research interests include channel coding, modulation, and wireless communications.

XING Wang received the B.S. degree from University of Science and Technology Beijing, China in 2019. He is currently pursuing the Ph.D. degree at the Wireless Communication Research Center, Institute of Computing Technology, Chinese Academy of Sciences. His current research interests include orthogonal time frequency space modulation and the convergence of communication, computation, and caching.

YUAN Jinhong received the B.E. and Ph.D. degrees in electronics engineering from the Beijing Institute of Technology, China, in 1991 and 1997, respectively. In 2000, he joined the School of Electrical Engineering and Telecommunications, University of New South Wales, Australia, where he is currently a professor and Head of Telecommunication Group with the School. He has published two books, five book chapters, over 300 papers in telecommunications journals and conference proceedings, and 50 industrial reports. He is a co-inventor of one patent on MIMO systems and two patents on low-density-parity-check codes. He has co-authored four Best Paper Awards and one Best Poster Award. He is an IEEE Fellow and currently serving as an Associate Editor for the *IEEE Transactions on Wireless Communications*. He served as the IEEE NSW Chapter Chair of Joint Communications/Signal Processions/Ocean Engineering Chapter during 2011-2014 and served as an Associate Editor for the *IEEE Transactions on Communications* during 2012-2017. His current research interests include error control coding and information theory, communication theory, and wireless communications.

ZHOU Yiqing received the B.S. degree in communication and information engineering and the M.S. degree in signal and information processing from Southeast University, China in 1997 and 2000, respectively, and the Ph.D. degree in electrical and electronic engineering from The University of Hong Kong, China in 2004. She is currently a professor with the Wireless Communication Research Center, Chinese Academy of Sciences. She has published over 150 articles and four books/book chapters. She received the best paper awards from WCSP2019, IEEE ICC2018, ISCIT2016, PIMRC2015, ICCS2014, and WCNC2013. She also received the 2014 Top 15 Editor Award from *IEEE TVT* and the 2016 – 2017 Top Editors of *ETT*. She is also the TPC Co-Chair of ChinaCom2012, an Executive Co-Chair of IEEE ICC2019, a Symposia Co-Chair of ICC2015, a Symposium Co-Chair of GLOBECOM2016 and ICC2014, a Tutorial Co-Chair of ICCC2014 and WCNC2013, and the Workshop Co-Chair of SmartGridComm2012 and GlobeCom2011. She is also the Associate/Guest Editor of some renowned journals.